https://doi.org/10.5194/egusphere-2025-5242
Preprint. Discussion started: 12 November 2025

Influences of CO_2 and Fungus-Assisted Bioweathering on Fluoridated Apatite

Mu Su[1,2#], Yuyang Cao[2#], Lingyi Tang[2#], Haoyang Weng[2#], Xiaoqing Shao[2], Zhijun Wang[2], Gilberto de Oliveira Mendes[3], Lingzi Meng[2], Meiyue Xu[2], Kun He[4*], Zibo Li[1], Mao Luo[1], Geoffrey Michael Gadd[5], Zhen Li[2*]

[1]*State Key Laboratory of Palaeobiology and Stratigraphy, Nanjing Institute of Geology and Palaeontology, Chinese Academy of Sciences, Nanjing 210008, China*

[2]*College of Resources and Environmental Sciences, Nanjing Agricultural University, Nanjing, Jiangsu 210095, China*

[3]*Laboratório de Microbiologia e Fitopatologia, Instituto de Ciências Agrárias, Universidade Federal de Uberlândia, Monte Carmelo, MG, Brazil*

[4]*Key Laboratory of Petroleum Geochemistry, Research Institute of Petroleum Exploration and Development, China National Petroleum Corporation, Beijing 100083, China*

[5]*Geomicrobiology Group, School of Life Sciences, University of Dundee, Dundee DD1 5EH, Scotland, UK*

[#]These authors contributed equally to this work

Corresponding author: Zhen Li (lizhen@njau.edu.cn)

https://doi.org/10.5194/egusphere-2025-5242
Preprint. Discussion started: 12 November 2025

Abstract

Fluoridated apatite (FAP) is the dominant P source for ecosystems. However, the bioweathering of FAP is still not fully elucidated. In this study, phosphate-solubilizing fungus *(Aspergillus niger*) was firstly incubated in soil to examine the weathering of FAP, on both cross and longitudinal sections. It showed that the fungus induced more pronounced erosion channels on the cross sections in a P-deficient soil. We therefore aimed to disentangle the relative contributions of biological (phosphate-solubilizing fungus) and abiotic factors (CO_2 and crystal face orientation) to the observed weathering contrasts. To further investigate the weathering contrasts on different sections of FAP, incubation was conducted in a culture medium. Fungal colonization on the cross section of FAP resulted in deeper P depletion zones and enriched secondary minerals (primarily calcium oxalate) than those on the longitudinal section. Additionally, elevated CO_2 (10%) significantly accelerated the weathering of FAP on the cross section, which was confirmed by its enhanced surface roughness, further promoted fungal colonization and subsequent bioweathering for FAP. Synergistic interactions between fungi and elevated CO_2 accelerate phosphate mineral weathering, providing a new insight on P cycling in soil microenvironments such as the rhizosphere.

Key words: Fungal bioweathering; Apatite; Elevated CO_2; Cross section; Hyphal-mineral interface

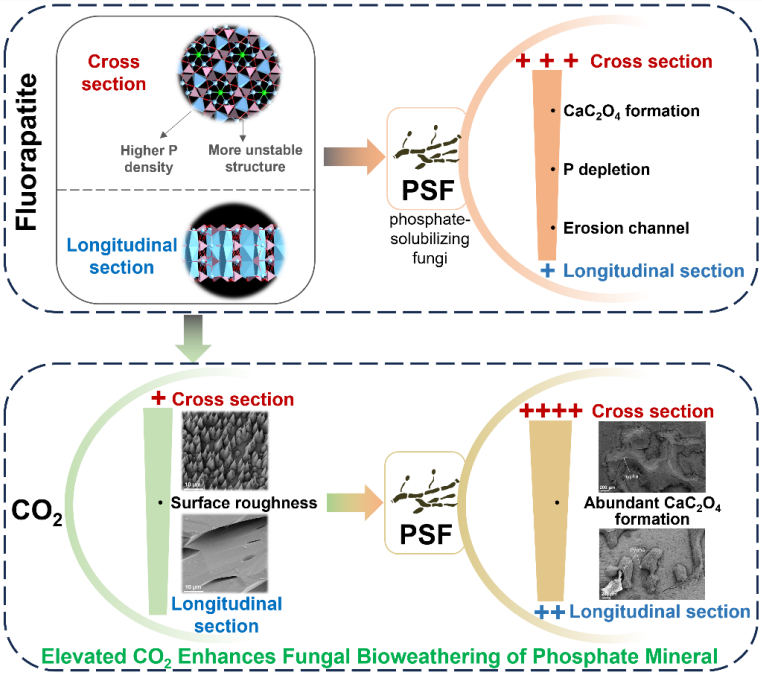

https://doi.org/10.5194/egusphere-2025-5242
Preprint. Discussion started: 12 November 2025

1. Introduction

Phosphorus is a key element in the replication, structural composition and metabolism of biomolecules (Elser, 2012). However, organisms are generally limited by available P in natural ecosystems (Elser et al., 2007; Meng et al., 2024). Therefore, P sets the pace of terrestrial and marine biological productivity on geological timescales (Tyrrell, 1999). FAP provides primary P for ecosystems via weathering (Chapin et al., 2011; Gadd, 2017). The delicate changes in apatite (the largest P inventory on Earth) weathering may significantly affect P availability in ecosystems on geological timescales.

Fungi can accelerate weathering of phosphate minerals through a series of growth and metabolic strategies (Hoffland et al., 2004; Rawat et al., 2021). For instance, phosphate-solubilizing fungi (PSF) can dissolve phosphate minerals via secreting proton and metabolic products (i.e., organic acids and siderophores) (do Nascimento et al., 2021; Mendes et al., 2021; Rawat et al., 2021). Filamentous fungi can also accelerate mineral destruction via hyphal osmotic pressure (Bonneville et al., 2016; Bonneville et al., 2009). Complementary processes allow the filamentous PSF to substantially erode phosphate minerals (Hoffland et al., 2004; Smits et al., 2012).

CO_2 is a crucial abiotic factor influencing FAP weathering. Dissolved CO_2 can induce formation of carbonic acid, which enhances the apatite dissolution by providing additional protons (Filippelli, 2008). In some natural environments, CO_2 concentration can be very high. For example, rhizosphere and similar microbial habitats often exhibit 10-100 times higher CO_2 than atmosphere from root and microbial respiration (Drever, 1994). Similarly, confined microenvironments such

https://doi.org/10.5194/egusphere-2025-5242
Preprint. Discussion started: 12 November 2025

as soil pores, fungal mats, or decaying organic-rich sediments may accumulate elevated CO_2, leading to locally acidified conditions. Elevated CO_2 not only promotes chemical dissolution of apatite but also alters microbial activity and growth patterns (Bertoloni et al. 2006; Schulz et al. 2012). The interplay between CO_2-driven geochemical reactions and CO_2-mediated microbial responses may strongly regulate apatite weathering in localized niches, yet this coupled mechanism remains poorly constrained.

Weathering of apatite is also regulated by mineralogical properties (Bogomolova et al., 2003). The weathering rates on different sections of a mineral could be distinct because of different bond values or hydration energies (Mkhonto and de Leeuw, 2002; Ruiz-Agudo and Putnis, 2012). Different sections of FAP crystals have distinct structures and atomic arrangements (Figs. S1a, b) (Elliott, 2002; Ichijo et al., 1992). In the FAP cross section (C_{FAP}), the Ca, P, F are arranged as the units of hexagons (Fig. S1a), while in the FAP longitudinal section (L_{FAP}), they form a unit of rectangle (Fig. S1b). The P densities in the C_{FAP} and L_{FAP} are 7.8 and 7.1 P atom exposed per nm^{-2} (Ichijo et al., 1992). The difference in surface elemental distribution results in higher proportion of P atoms (40% of P atoms in the total number of atoms) in C_{FAP} compared to L_{FAP} (25%). In addition, orientation within mineral crystals may influence chemical stability and mechanical resistance (Giri et al., 2012). Different crystal planes of the mineral showed distinct elemental composition (Gleeson et al., 2005; Ichijo et al., 1992) and surface properties (e.g., porosity, microtopography, surface charge, hydrophobicity) (Bogomolova et al., 2003), which would influence microbial growth on mineral surfaces (Zhang et al., 2021). To maximize nutrient and minimize energy consumption, microorganisms selectively attach onto mineral surfaces

https://doi.org/10.5194/egusphere-2025-5242
Preprint. Discussion started: 12 November 2025

containing growth-limiting nutrients, (i.e., P, N) (Rogers et al., 1998). Cell adhesion to minerals was usually correlated with particular element site density (Neal et al., 2005). In addition, microorganisms have a strong tendency to grow along surface cracks and junctions between crystals (Bogomolova et al., 2003). However, the contrasts of fungal bioweathering on the different sections of FAP have not been elucidated.

The aim of this study was to investigate how elevated CO_2 and *A. niger* affect FAP weathering. The effect of fungal colonization and CO_2 concentration on weathering C_{FAP} and L_{FAP} was explored.

2. Materials and Methods

2.1 Fungal Strain Preparation

The *Aspergillus niger* (CCTCC No. M2023240) was applied in this study. *A. niger* was cultured on potato dextrose agar (PDA) medium at 28 °C for 5 d to produce spores. The PDA medium had 5 g/L potato infusion, 20.0 g/L glucose, and 14.0 g/L agar. The medium was drenched with sterile water and the spores were carefully scraped from the plate surface with a fine artist's brush. The suspension was then filtered through a three-layer sterile cheesecloth to eliminate mycelial fragments.

2.2 Preparation of FAP

Durango fluorapatite (FAP) was considered as a standard geological apatite. The FAP was sectioned into 200 μm thick, 0.5 cm × 0.5 cm slices with cross sections (Figs. S1A and S1C) and longitudinal sections (Figs. S1B and S1C). The longitudinal section of an appetite slice was cut along the edges of the unit cell. All FAP slices were stored in a desiccator prior to the following

https://doi.org/10.5194/egusphere-2025-5242
Preprint. Discussion started: 12 November 2025

experiments. A three-dimensional structure of the apatite cross and longitudinal sections is shown in Fig. S1A and Fig. S1B, respectively.

2.3 Bioweathering of FAP in Soil

Bioweathering of FAP by *A. niger* was first conducted using P-deficient soil. The P-deficient soil sample (0–20 cm) was collected from Chongzuo, Guangxi, China. The soil was acidic (pH 4.95) and contained only 0.53 mg Kg^{-1} of available P. Soil sample was sieved (2 mm mesh) to remove roots and gravel. Then 20 g dry soil was placed in a 50 mL glass bottle. After sterilization at 121 °C for 1 h, each bottle content was evenly sprayed with 1 mL sterile solution (containing 0.7 g of C and 0.028 g of N per week per kg dry soil). Subsequently, 1 mL *A. niger* spore suspension (4.3×10^7 spores mL^{-1}) was inoculated into the soil. Afterwards, two ultraviolet-sterilized glass sheets with attached FAP samples (cross and longitudinal sections) were inserted vertically into the soil. These two treatments were denoted as CPSF@Soil and LPSF@Soil. Each treatment was performed with two experimental replicates. The bottles were incubated in the dark at 25 °C (60% of maximum soil water-holding capacity). After 30 d incubation, two FAP slices were cleaned using sterile water and air dried at room temperature for SEM analysis.

2.4 Weathering of FAP in Medium

(i) Weathering of FAP by PSF: To further investigate the factors causing differences in the weathering rates of different apatite crystal facets, a set of experiments was conducted in PDA medium. Two ultraviolet-sterilized glass sheets with attached FAP samples were vertically inserted into the PDA medium. Then, 0.1 mL of *A. niger* spore suspension (4.3×10^7 spores mL^{-1}) was inoculated. The FAP slices with *A. niger* inoculation were incubated at 28 °C under sterile ambient

https://doi.org/10.5194/egusphere-2025-5242
Preprint. Discussion started: 12 November 2025

air for 45 d, which were denoted as CPSF (cross section with *A. niger*) and LPSF (longitudinal section with *A. niger*) treatments (Fig. S1D). Each treatment was performed with two experimental replicates. Two FAP slices were then cleaned using sterile water and air dried at room temperature for SEM-EDS, Raman imaging and scanning electron microscopy (RISE) analysis. In addition, FAP with growing hyphae were protected by deposition of a platinum strap (~1 mm thick). Then, focused ion beam (FIB) was applied to prepare hypha-mineral interface profiles (~90 nm thick) for transmission electron microscopy-energy dispersive spectroscopy (TEM-EDS) analysis.

(ii) Weathering of FAP by elevated CO_2: FAP slices were also prepared without PSF addition and incubated at 10% CO_2 concentration (denoted as C_{FAP}@CO_2 and L_{FAP}@CO_2 treatments) to investigate the effects of sole CO_2 on apatite weathering. Each treatment was performed with two experimental replicates. After 45 d incubation, FAP slices were gently rinsed using sterile water and air dried at room temperature for scanning electron microscopy and atomic force microscopy (AFM).

(iii) Weathering of FAP by PSF and elevated CO_2: To examine the synergistic effect of fungal colonization and elevated CO_2 on apatite weathering, another two glass sheets attached FAP samples with PSF addition were incubated in an incubator containing 10% CO_2 (denoted as CPSF@CO_2 and LPSF@CO_2 treatments). Each treatment was performed with two experimental replicates. After 45 d incubation, two FAP slices were cleaned using sterile water and air dried at room temperature for SEM analysis.

2.5 Instrumentation

SEM image analysis was performed using a Carl Zeiss Supra 55 system (Carl Zeiss Inc.,

https://doi.org/10.5194/egusphere-2025-5242
Preprint. Discussion started: 12 November 2025

Germany) in secondary electron imaging mode with an acceleration voltage of 7-15 kV. To enhance image quality and minimize charging, samples were sputter-coated with gold for SEM analysis. To ensure representation, the regions scanned were selected randomly. Semi-quantitative analysis (collecting time: 60 s) was performed using an Oxford Aztec X-Max 150 energy dispersive spectrometer (EDS).

RISE system consisted of a Wissen schaftliche Instrumente and Technologie GmbH (WITech, Germany) Alpha 300 confocal Raman microscope combined with an SEM (TESCAN-VEGA3). The spectral region of 0–4500 cm^{-1} was recorded using a 532 nm laser (15 mW with 4×15 s scans). In addition, Raman spectra of P-O (for PO_4^{3-} in apatite slice) vibration were collected using a Horiba Lab RAM HR Evolution instrument equipped with an Olympus microscope. The instrument was calibrated using a silicon wafer at band position of 520.7 cm^{-1}. Then, the spectral region of 400–1500 cm^{-1} was recorded using a 633 nm laser (4 mW with 2 ×60 s scans).

Hypha-apatite interface profiles were prepared and polished using Zeiss Crossbeam 550 FIB-SEM. Polished samples were then analyzed using TEM-EDS (deadtime: 90 s). TEM was performed using FEI Tecnai G2 F20 system. Semi-quantitative analysis (collecting time: 40 s) was performed using an Oxford Aztec X-Max 150 EDS.

AFM measurement was carried out using a Bruker Dimension Icon scanning probe microscope at room temperature. The PeakForce Tapping mode was utilized for all AFM measurements. The tip (Bruker, TAP150A) had a half cone angle of 10°, a radius of 10 nm, and a resonance frequency of 150 kHz. The nominal force constant was 5 N/m and the actual spring constant of the probe was calibrated before each test.

https://doi.org/10.5194/egusphere-2025-5242
Preprint. Discussion started: 12 November 2025

2.6 Data Analysis

Effects of elevated CO_2 on the surface roughness of FAP cross and longitudinal sections were evaluated by comparing C_{FAP}@CO_2 and L_{FAP}@CO_2 treatments. Data was tested for normality and homogeneity of variances and then analyzed by a One-way analysis of variance at a significance level of $P < 0.05$. All statistical analyses were conducted in R software (version 4.3.2; R Core Team, 2023). The 3D structural diagram of apatite sections was examined by CrystalMaker 10.4.

3. Results

3.1 Fungal-induced Surface Dissolution and Secondary Mineral Formation on FAP

Hyphae extended to FAP surfaces in soil experiments, with deep channels forming along hyphae in CPSF@Soil (Figs. 1a, c) while none forming in LPSF@Soil (Figs. 1b, d). For the incubation in the medium, more fungal mycelia were observed in CPSF compared with LPSF (Figs. 2a, b). Abundant secondary minerals formed around mycelium on both sections (Figs. 2c, e, d, f), with more bipyramid-shaped minerals on C_{FAP} (Fig. 2c). EDS analysis showed intense C, O, and Ca signals in these secondary minerals. Based on their morphology, these minerals resembled calcium oxalate (Mendes et al., 2022).

RISE analysis was applied to determine the phase of secondary minerals on the FAP surface. The peak at 968 cm^{-1} corresponded to the ν_1 stretching vibration of P-O from PO_4^{3-} (Fig. S2). The 1488 cm^{-1} peak was assigned to ν (C-O) vibrations of oxalate (Su et al., 2023). In the spot analysis on initial C_{FAP} and L_{FAP}, only the characteristic peaks of phosphate were observed (Fig. S2). After incubation, the characteristic peaks of oxalates were detected on the rhomboid-shaped secondary

https://doi.org/10.5194/egusphere-2025-5242
Preprint. Discussion started: 12 November 2025

minerals on both sections (Fig. S2).

3.2 Fungal Influence on Ca and P Migration on the FAP Surface

Raman spectra showed the intense P-O signal on the FAP surfaces in both CPSF and LPSF treatments (Figs. 3a, b). The peaks at 429, 446 cm^{-1} were assigned to ν_2 P-O vibrations, those at 582, 605 cm^{-1} to ν_4, the peak at 963 cm^{-1} to ν_1, and those at 1032, 1058, 1078 cm^{-1} to ν_3 P-O vibrations. The peaks at 446, 1032, 1058, 1078 cm^{-1} were only observed on the C_{FAP} (Fig. 3a), while the characteristic peak at 429 cm^{-1} was only observed on the L_{FAP} (Fig. 3b). Additionally, on the C_{FAP}, the P-O peaks (e.g., 582, 605, 1032, 1058, 1078 cm^{-1}) exhibited higher intensities 20 µm from the hypha (point a1) than at 2 µm (point a2) (Fig. 3a; Table S1). The characteristic peaks of P-O remained consistent on the L_{FAP} (Fig. 3b).

FIB-prepared hyphal-mineral interface profiles detected altered Ca and P atomic content (Figs. 3c, d, e). At 0.03 µm depth from the hyphal-mineral interface, Ca and P contents on C_{FAP} were only 3.5% and 2.3% (Fig. 3c), versus 4.9% and 6.4% on L_{FAP} (Fig. 3d). The atomic contents of Ca and P in both profiles increased rapidly from the hyphal-mineral interface to a depth of 0.1 µm, where they reached 12.4% and 9.1% for the C_{FAP}, 15.7% and 13.0% for the L_{FAP}. Ca and P contents stabilized at 19.6% and 14.3% at 3.2 µm depth in C_{FAP}, versus 20.7% and 15.7% at 1.7 µm in L_{FAP}. In contrast to L_{FAP}, the contents of Ca and P at the same depth in the C_{FAP} were lower (Figs. 3c, d). EDS analysis showed that the Ca/P ratios in the C_{FAP} profile was always higher than that in the L_{FAP} profile within a depth of 0.32 µm from the hyphal-mineral interface. Then, the Ca/P ratios tended to be constant (~1.3) in both the profiles (Fig. 3e).

3.3 CO_2-induced Alteration of FAP Surface Roughness

https://doi.org/10.5194/egusphere-2025-5242
Preprint. Discussion started: 12 November 2025

Both C_{FAP} and L_{FAP} exhibited relatively smooth surfaces before incubation (Figs. 4a, c). Elevated CO_2 exposure produced abundant sharp hexagonal columnar structures (2-3 μm diameter) on C_{FAP} (Fig. 4b), while produced trench-like structures on L_{FAP} (Fig. 4d). Initial C_{FAP} step height varied -2 to 3 nm (Fig. 4e), expanding to -9-9 nm after elevated CO_2 incubation (Fig. 4f). In contrast, the step height variation for the L_{FAP} ranged from -6 to 6 nm (Figs. 4g, h). Elevated CO_2 significantly increased the surface roughness of the C_{FAP} (from 2.8 to 5.4 nm), while had limited effect on the surface of L_{FAP} (Fig. 4i).

3.4 Synergistic Effects of CO_2 and Fungi on FAP Weathering

Abundant hexagonal columnar structures were formed on the surface of C_{FAP} in the CPSF@CO_2 treatment (Fig. 5a). However, the sharpness of the columnar structures was reduced compare with that in the C_{FAP}@CO_2 treatments (Fig. 4b). For the L_{FAP}, elevated CO_2 and PSF synergistically induced additional cracks in LPSF@CO_2 (Fig. 5d). Compared with L_{FAP}, 40.2 mm^2 more secondary mineral areas were formed on the surface of C_{FAP} (Fig. S3). These secondary mineral areas were mainly composed of calcium oxalate particles (Figs. 5b, e). Calcium oxalate particles predominantly accumulated along hyphae on C_{FAP} (Fig. 5c), whereas on L_{FAP} they exhibited scattered low-density aggregation (Fig. 5f).

4. Discussion

The different sections of FAP are significantly different in elemental distribution (Figs. S1a, b) and structural stability. The Ca, P, and F are arranged as the units of hexagons in the C_{FAP} (Fig. S1a), while forming a unit of rectangle in the L_{FAP}. The difference in surface elemental distribution results in a higher proportion of P atoms (40% of P atoms in the total number of atoms) in C_{FAP}

https://doi.org/10.5194/egusphere-2025-5242
Preprint. Discussion started: 12 November 2025

compared to L_{FAP} (25%). In addition, the screw dislocation of atoms often causes surface defects of crystal, which further reduces the structural stability of mineral crystals. Since the screw dislocation of atoms often occurs in the cross section of the crystal (Cuisinier et al., 1992), C_{FAP} may have lower resistance to weathering than L_{FAP}. These differences in elemental distribution and structural stability between C_{FAP} and L_{FAP} may further influence weathering of FAP.

A. niger induced more P depletion zones on the C_{FAP} (Figs. 3a, c), suggesting that C_{FAP} is more vulnerable to fungal weathering than L_{FAP}. PSF usually grow and expand their hyphae on the surface of minerals to obtain nutrients (Gadd, 2010). The relatively high P density in C_{FAP} may lead to the preferential growth of fungal hyphae. The low P content and high Ca/P ratio (Fig. 3e) at the mycelia-FAP interface further suggest that the P acquisition by *A. niger* may cause stronger biological weathering in C_{FAP}. Fungal hyphae can accelerate the weathering of FAP via the following two pathways. First, organic acids released from the TCA cycle accelerate the solubilization of apatite mineral (Rawat et al., 2021; Su et al., 2021). Oxalic acid, the most abundant organic acid secreted by *A. niger* have higher acidity constants than many other organic acids (Zhang et al., 2021). Given the low structural stability of C_{FAP}, H^+ and organic acid ligands drive preferential bioweathering. Oxalic acid can react with Ca^{2+} dissolved from FAP, the formation of calcium oxalate therefore can be applied to evaluate such fungal bioweathering processes (Sturm et al., 2015; Su et al., 2021). The results that more calcium oxalate were formed near the mycelium on the C_{FAP} than L_{FAP} (Figs. 2c, d), further confirmed that the bioweathering of C_{FAP} is stronger than that of L_{FAP}. Second, *A. niger* can also accelerate the physical destruction of FAP through the biomechanical forces of mycelium growth. Fungal appressoria can produce

https://doi.org/10.5194/egusphere-2025-5242
Preprint. Discussion started: 12 November 2025

osmotic pressures of up to 10–20 $\mu N/\mu m^2$ during hyphal growth, which would substantially accelerate the physical weathering (Hoffland et al., 2004; Howard et al. 1991). Screw dislocations in crystal cross-sections destabilize C_{FAP} structure, enhancing its susceptibility to biomechanical destruction. Moreover, the released fluorine from FAP did not cause evident toxicity on the mineral surface.

CO_2 can form carbonic acid in humid environments, resulting in FAP weathering. In this study, elevated CO_2 induced the formation of hexagonal pyramids and trench-like structures (Figs. 4a, b, c, d) on FAP surfaces and increased the roughness on C_{FAP} surface (Figs. 4e, f, i). This suggests that abiotic factors also preferably weather C_{FAP}. In addition, the decreased sharpness of the columnar structure on the C_{FAP} and more cracks on the L_{FAP} after fungal inoculation indicated that the PSF would survive and perform its solubilizing ability under elevated CO_2 (Figs. 5a, d). These observations highlight that elevated CO_2 not only accelerates chemical dissolution but also sustains fungal colonization and activity on mineral surfaces.

Elevated CO_2 can promote surface roughness of FAP, especially on CFAP, which provides more favorable habitats for the spores and hyphae of PSF. Such roughened surfaces may facilitate adhesion, enhance hyphal penetration, and stimulate oxalic acid secretion by PSF, further promoting bio-weathering. The synergistic effect of fungal colonization and high CO_2 concentration on FAP weathering has many important implications. In soils, rhizosphere serves as the crucial zone for P transfer from the lithosphere to the biosphere, which mediates crucial P transfer from lithosphere to biosphere. Rhizosphere zones often maintain CO_2 levels several-fold higher than the atmosphere due to intense root and microbial respiration, with values up to ~4%

https://doi.org/10.5194/egusphere-2025-5242
Preprint. Discussion started: 12 November 2025

(Drever, 1994). Beyond bulk rhizosphere CO_2 enrichment, fungal hyphae themselves can locally elevate CO_2 concentrations and simultaneously reduce O_2, creating steep microscale gradients. These self-generated microenvironments may alter surface chemistry, increase mineral roughness, and promote stable colonization, thereby amplifying fungal bio-weathering at the μm scale. While traditional views hold that exudates (e.g., simple carbohydrates) in rhizosphere stimulate microbial growth—enhancing decomposer community nutrient cycling, our findings under controlled conditions are thus consistent with processes expected in natural soils, where abiotic and biotic drivers interact to regulate P release, which provides a new insight into rhizosphere P transformation processes. In addition, our results also consistently showed that both abiotic and biotic weathering processes predominately occurred in the cross section of FAP. Given that approximately ~90% of P is stored in the form of apatite on the earth (Chapin et al., 2011), the preferential weathering of CFAP observed in both abiotic and biotic contexts underscores the need to consider crystal face-specific processes in future studies. Linking microscale fungal–CO_2 interactions with larger-scale geochemical cycling will be essential for more accurate predictions of terrestrial and marine P dynamics.

5. Conclusions

Fungal colonization and high CO_2 concentration synergistically promoted FAP weathering. Fungal colonization boosted oxalic acid production and induced P depletion zones. Elevated CO_2 enhanced surface roughness which promoted fungal adhesion and growth, further accelerated bioweathering of FAP. These indicate that the P cycling in soil microenvironments with higher CO_2 concentrations (like in the rhizosphere) may be faster. In addition, the alterations of

https://doi.org/10.5194/egusphere-2025-5242
Preprint. Discussion started: 12 November 2025

morphology and elemental composition in the mycelial-mineral interfaces indicate that both abiotic and biotic weathering processes preferentially occurred in C_{FAP}. Given that approximately 90% of P is stored in the form of apatite on the Earth, future studies should pay more attention to weathering processes at the different faces of FAP crystals, for accurately predicting P cycling in terrestrial and marine ecosystems.

Data Availability Statement

The data that support the findings of this study are openly available in Zenodo digital repository (https://doi.org/10.5281/zenodo.17382598)

Author contributions

MS: Writing-original draft, Data curation, Visualization, Methodology, Investigation, Formal analysis, Conceptualization, Funding acquisition. YC, LT and HW: Data curation, Visualization, Methodology, Investigation, Formal analysis, Conceptualization. XS and ZW: Methodology, Investigation. LM and MX: Methodology. GM, KH, ZbL, ML and GG: Writing-review and editing, Methodology, Investigation, Formal analysis, Conceptualization. ZL: Writing-review and editing, Resources, Methodology, Investigation, Funding acquisition, Formal analysis, Conceptualization.

Competing Interest

The authors declare that they have no known competing financial interests or personal relationships that could have appeared to influence the work reported in this paper.

Acknowledgements

This study was supported by National Natural Science Foundation of China (42403075), National Key R&D Program of China (2023YFC3707600), the Major Scientific and Technological Project

https://doi.org/10.5194/egusphere-2025-5242
Preprint. Discussion started: 12 November 2025

of CNPC (2023ZZ0203) and China Postdoctoral Science Foundation (2024M753324).

References

Bertoloni, G., Bertucco, A., De Cian, V. Parton, T. (2006). A study on the inactivation of micro-organisms and enzymes by high pressure CO_2 . Biotechnology and Bioengineering, 95, 155-160.

Bogomolova, E.V., Olkhovaya, E.A., Panina, L.K. and Soukharjevsky, S.M. (2003) Experimental study of influence of rocks and minerals chemical composition and surface structure over the lithobiontic fungi colonies morphology. Mikol Fitopatol 37, 1-13.

Bonneville, S., Bray, A.W. and Benning, L.G. (2016) Structural Fe(II) Oxidation in Biotite by an Ectomycorrhizal Fungi Drives Mechanical Forcing. Environmental Science and Technology. 50, 5589-5596.

Bonneville, S., Smits, M.M., Brown, A., Harrington, J., Leake, J.R., Brydson, R. and Benning, L.G. (2009) Plant-driven fungal weathering: Early stages of mineral alteration at the nanometer scale. Geology 37, 615-618.

Chapin, F.S., Matson, P.A. and Vitousek, P.M. (2011) Changes in the Earth System, in: Chapin, F.S., Matson, P.A., Vitousek, P.M. (Eds.), Principles of Terrestrial Ecosystem Ecology, Second ed. Springer, pp. 401-422.

Cuisinier, F.J.G., Steuer, P., Senger, B., Voegel, J.C. and Frank, R.M. (1992) Human amelogenesis I: High resolution electron microscopy study of ribbon-like crystals. Calcified Tissue International 51, 259-268.

Drever, J.I. (1994) The effect of land plants on weathering rates of silicate minerals. Geochimica et Cosmochimica Acta 58, 2325-2332.

Do Nascimento, J. M., Netto, J. A. F. V., Valadares, R. V., Mendes, G. D., da Silva, I. R., Vergutz, L., & Costa, M. D. (2021). *Aspergillus niger* as a key to unlock fixed phosphorus in highly weathered soils. Soil Biology and Biochemistry, 156, 108190.

Elliott, J.C. (2002) Calcium phosphate biominerals, in: Kohn, M.J., Rakovan, J., Hughes, J.M. (Eds.),

https://doi.org/10.5194/egusphere-2025-5242
Preprint. Discussion started: 12 November 2025

Phosphorus: Geochemical, Geobiological, and Materials Importance, pp. 427–453.

Elser, J.J. (2012) Phosphorus: a limiting nutrient for humanity? Current opinion in biotechnology 23, 833-838.

Elser, J.J., Bracken, M.E.S., Cleland, E.E., Gruner, D.S., Harpole, W.S., Hillebrand, H., Ngai, J.T., Seabloom, E.W., Shurin, J.B. and Smith, J.E. (2007) Global analysis of nitrogen and phosphorus limitation of primary producers in freshwater, marine and terrestrial ecosystems. Ecology Letters 10, 1135-1142.

Filippelli, G.M. (2008) The global phosphorus cycle: Past, present, and future. Elements 4, 89-95.

Gadd, G.M. (2010) Metals, minerals and microbes: geomicrobiology and bioremediation. Microbiology 156, 609-643.

Gadd, G.M. (2017) The geomycology of elemental cycling and transformations in the environment. Microbiology spectrum 5, 1-16.

Giri, B., Almer, J.D., Dong, X.N. and Wang, X.D. (2012) In situ mechanical behavior of mineral crystals in human cortical bone under compressive load using synchrotron X-ray scattering techniques. Journal of the Mechanical Behavior of Biomedical Materials 14, 101-112.

Gleeson, D.B., Clipson, N., Melville, K., Gadd, G.M. and McDermott, F.P. (2005) Characterization of fungal community structure on a weathered pegmatitic granite. Microbial Ecology 50, 360-368.

Hoffland, E., Kuyper, T.W., Wallander, H., Plassard, C., Gorbushina, A.A., Haselwandter, K., Holmstrom, S., Landeweert, R., Lundstrom, U.S., Rosling, A., Sen, R., Smits, M.M., van Hees, P.A. and van Breemen, N. (2004) The role of fungi in weathering. Frontiers in Ecology and the Environment 2, 258-264.

Howard RJ, Ferrari MA, Roach DH, and Money NP. 1991. Penetration of hard substrates by a fungus employing enormous turgor pressures. Proceedings of the National Academy of Sciences of the United States of America 88: 11281–84.

Ichijo, T., Yamashita, Y. and Terashima, T. (1992) Observations on the structural features and characteristics of biological apatite crystals. 2. Observation on the ultrastructure of human enamel crystals. The Bulletin of Tokyo Medical and Dental University 39, 71-80.

https://doi.org/10.5194/egusphere-2025-5242
Preprint. Discussion started: 12 November 2025

Mendes, G.D., Bahri-Esfahani, J., Csetenyi, L., Hillier, S., George, T.S. and Gadd, G.M. (2021a) Chemical and physical mechanisms of fungal bioweathering of rock phosphate. Geomicrobiology Journal 38, 384-394.

Mendes, G.D.O., Dyer, T., Csetenyi, L. and Gadd, G.M. (2021b) Rock phosphate solubilization by abiotic and fungal - produced oxalic acid: reaction parameters and bioleaching potential. Microbial Biotechnology 15, 1189-1202.

Meng, L.Z., Chen, Y.H., Tang, L.Y., Sun, X.Q., Huo, H.X., He, Y.X., Huang, Y.N., Shao, Q., Pan, S. and Li, Z. (2024) Effects of temperature-related changes on charred bone in soil: From P release to microbial community. Current Research in Microbial Sciences 6, 100221.

Mkhonto, D. and de Leeuw, N.H. (2002) A computer modelling study of the effect of water on the surface structure and morphology of fluorapatite: introducing a $Ca_{10}(PO_4)_6F_2$ potential model. Journal of Materials Chemistry 12, 2633-2642.

Neal, A.L., Bank, T.L., Hochella, M.F. and Rosso, K.M. (2005) Cell adhesion of Shewanella oneidensis to iron oxide minerals: Effect of different single crystal faces. Geochemical transactions 6, 77-84.

Rawat, P., Das, S., Shankhdhar, D. and Shankhdhar, S.C. (2021) Phosphate-solubilizing microorganisms: mechanism and their role in phosphate solubilization and uptake. Journal of Soil Science and Plant Nutrition 21, 49-68.

Rogers, J.R., Bennett, P.C. and Choi, W.J. (1998) Feldspars as a source of nutrients for microorganisms. American Mineralogist 83, 1532-1540.

Ruiz-Agudo, E. and Putnis, C.V. (2012) Direct observations of mineral fluid reactions using atomic force microscopy: the specific example of calcite. Mineralogical Magazine 76, 227–253.

Schulz, A., Vogt, C. Richnow, H.H. (2012). Effects of high CO_2 concentrations on ecophysiologically different microorganisms. Environmental Pollution, 169, 27-34.

Smits, M.M., Bonneville, S., Benning, L.G., Banwart, S.A. and Leake, J.R. (2012) Plant - driven weathering of apatite – the role of an ectomycorrhizal fungus. Geobiology 10, 445-456.

Sturm, E.V., Frank-Kamenetskaya, O., Vlasov, D., Zelenskaya, M., Sazanova, K., Rusakov, A. and Kniep, R. (2015) Crystallization of calcium oxalate hydrates by interaction of calcite marble with fungus

https://doi.org/10.5194/egusphere-2025-5242
Preprint. Discussion started: 12 November 2025

Aspergillus niger. American Mineralogist 100, 2559–2565.

Su, M. (2025). Data for "Influences of CO_2 and Fungus-Assisted Bioweathering on Fluoridated Apatite" [Data set]. Zenodo. https://doi.org/10.5281/zenodo.17382598.

Su, M., Mei, J.J., Pan, S., Xu, J.J., Gu, T.T., Li, Q., Fan, X.R. and Li, Z. (2023b) Raman spectroscopy to study biomolecules, their structure, and dynamics, in: Saudagar, P., Tripathi, T. (Eds.), Advanced Spectroscopic Methods to Study Biomolecular Structure and Dynamics. Elsevier, London, United Kingdom, pp. 173-198.

Su, M., Meng, L.Z., Zhao, L., Tang, Y.K., Qiu, J.J., Tian, D. and Li, Z. (2021) Phosphorus deficiency in soils with red color: Insights from the interactions between minerals and microorganisms. Geoderma 404, 115311.

Tyrrell, T., 1999, The relative influences of nitrogen and phosphorus on oceanic primary production. Nature, 400, 525-531.

Zhang, L., Gadd, G.M. and Li, Z. (2021) Microbial biomodification of clay minerals. Advances in Applied Microbiology 114, 111-139.

https://doi.org/10.5194/egusphere-2025-5242
Preprint. Discussion started: 12 November 2025

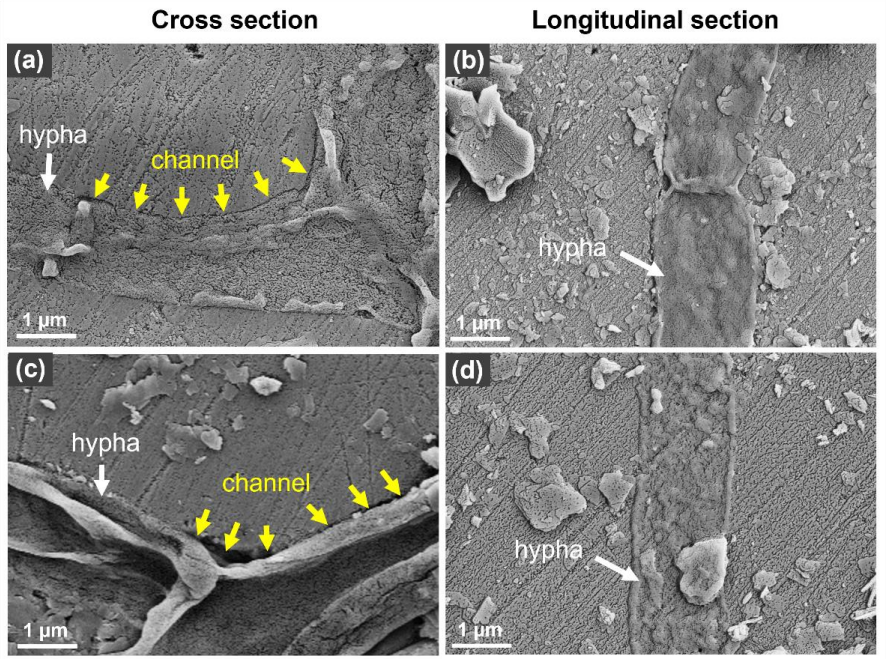

Figure 1. SEM imaging of *A. niger* hyphae on the FAP surface in the CPSF@Soil (a, c) and LPSF@Soil (b, d) treatments. The hyphae promote the formation of erosion channels (yellow arrow) on the FAP cross section (a and c).

https://doi.org/10.5194/egusphere-2025-5242
Preprint. Discussion started: 12 November 2025

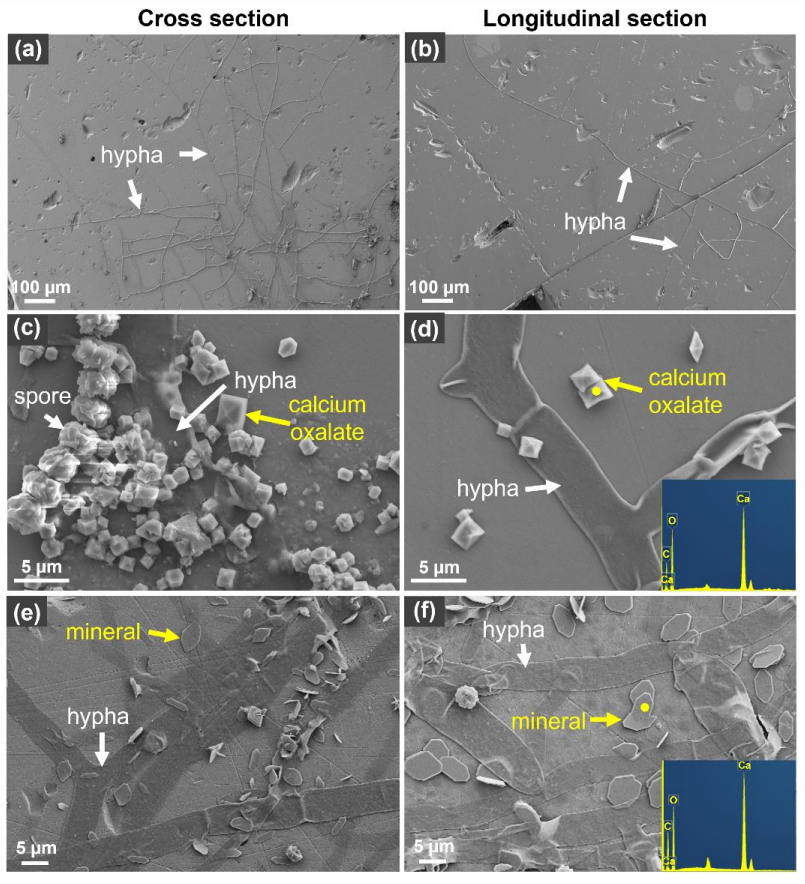

Figure 2. SEM imaging of *A. niger* hyphae and secondary minerals on the FAP surface in the CPSF (a, c, e) and LPSF (b, d, f) treatments.

https://doi.org/10.5194/egusphere-2025-5242
Preprint. Discussion started: 12 November 2025

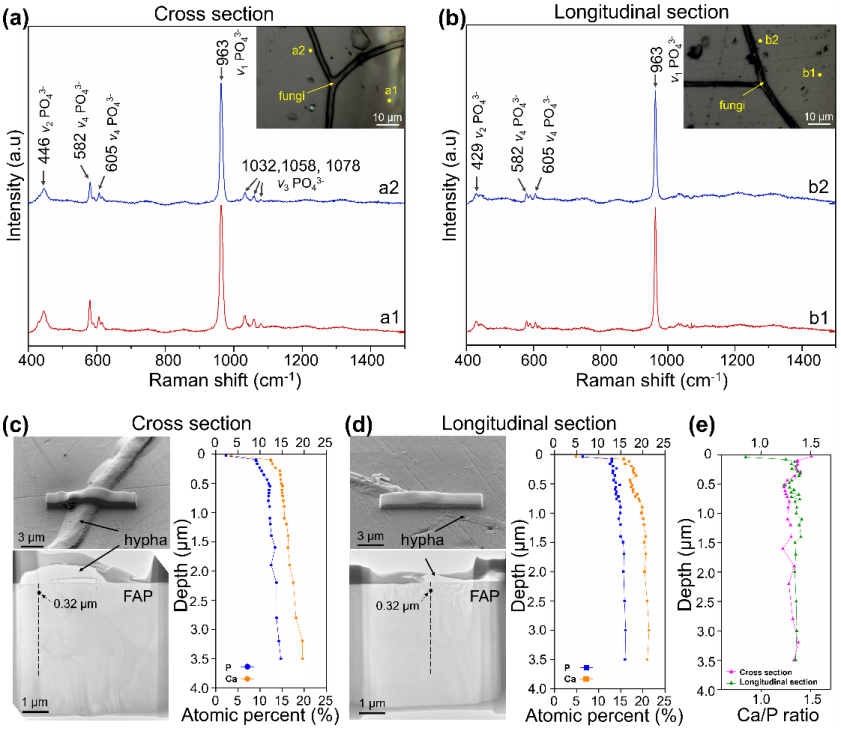

Figure 3. Raman spectra of P-O vibration on the FAP surface (a for CPSF and b for LPSF treatments) and normalized atomic percent of Ca and P in FIB-prepared hypha-mineral interface profiles (c for CPSF and d for LPSF treatments) and the corresponding Ca/P ratio in these profiles (e). a1, b1: ~20 μm away from the hypha; a2, b2: ~2 μm away from the hypha. The atomic percentage of Ca and P and Ca/P ratio are related to the points shown along the black dotted lines in Figure c and d. The contents of Ca and P showed obvious changes within 0.32 μm below the hypha-mineral interface.

https://doi.org/10.5194/egusphere-2025-5242
Preprint. Discussion started: 12 November 2025

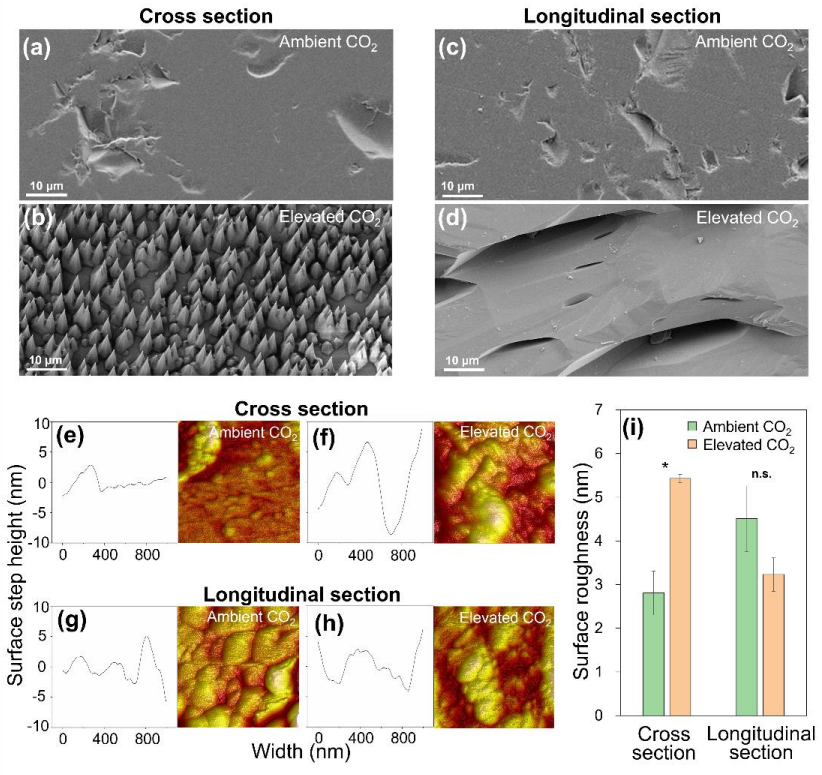

Figure 4. FAP surface morphology (a, b, c, d), surface step height (e, f, g, h), and surface roughness (i) in the C_{FAP}@CO_2 and L_{FAP}@CO_2. a and b: SEM images of the C_{FAP} surface at ambient (a) and elevated (b) CO_2 condition. c and d: SEM images of the L_{FAP} surface at ambient (c) and elevated (d) CO_2 condition. e-h: Surface step height of the C_{FAP} (e and f) and L_{FAP} (g and h) at ambient and elevated CO_2 condition. Images on the right are the atomic force microscope (AFM) height 3D image of FAP surface in the corresponding sites. i: The surface roughness (high sensor) of the FAP based on the AFM analysis. Values were presented as mean±standard error (n = 3, three different sites on one FAP section were analyzed). Asterisk (*) indicated significant difference ($P < 0.05$) of FAP surface roughness after etching by elevated CO_2, while n.s. indicated no significant difference.

https://doi.org/10.5194/egusphere-2025-5242
Preprint. Discussion started: 12 November 2025

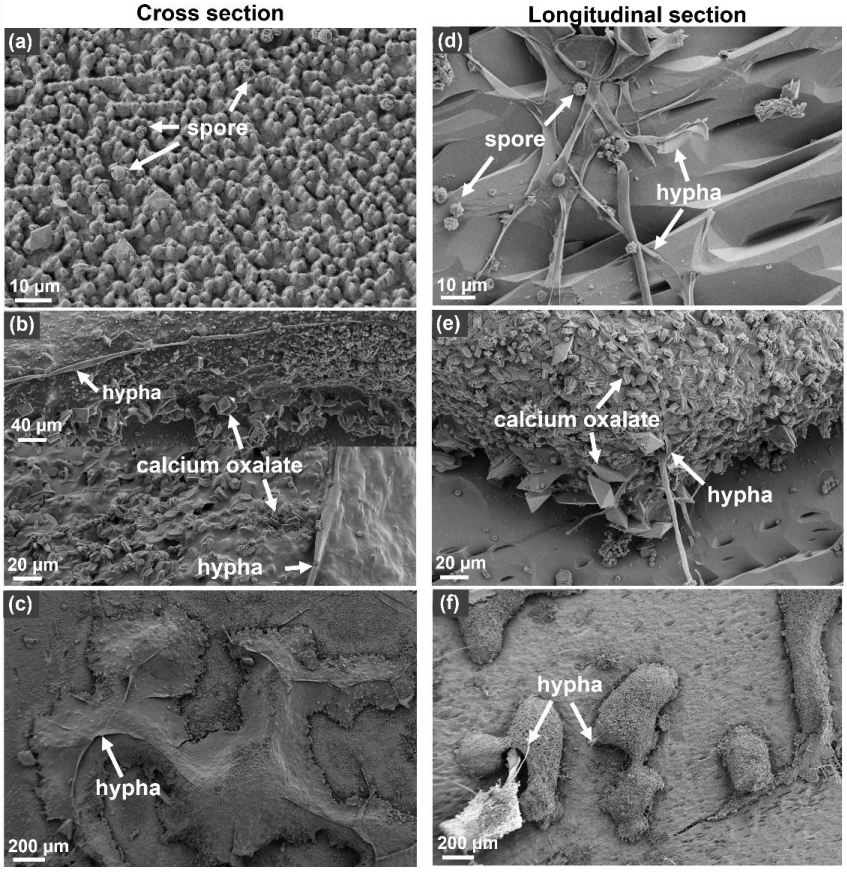

Figure 5. The morphology of the FAP surface and the calcium oxalate formed on it in the CPSF@CO_2 (a, b, c) and LPSF@CO_2 (d, e, f) treatments. a and d: abundant columnar structure with reduced sharpness were observed on the C_{FAP} surface (a) and induced additional cracks appeared on the L_{FAP} surface (d). b and e: two types of calcium oxalate on the FAP surface. c and f: Calcium oxalate accumulated along the hyphae on the C_{FAP} surface (c) and exhibited a scattered aggregation on the L_{FAP} surface (f).